Empirical models to describe UAV tonal dynamics during real operations

Andino Cappagli, C.I.; Amiri Simkooei, A.; Snellen, M.

Publication date
2024

Document Version
Final published version

Published in
QUIETDRONES 2024

QUIETDRONES 2024
MANCHESTER
8th - 11th September 2024

Empirical models to describe UAV tonal dynamics during real operations

Session: UAS/UAM Noise Prediction

Camilo Ignacio Andino Cappagli, Faculty of Aerospace Engineering, Delft University of Technology, Netherlands, c.i.andinocappagli@tudelft.nl
Alireza Amiri-Simkooei, Faculty of Aerospace Engineering, Delft University of Technology, Netherlands, a.amirisimkooei@tudelft.nl
Mirjam Snellen, Faculty of Aerospace Engineering, Delft University of Technology, Netherlands, m.snellen@tudelft.nl

Abstract Over the last decade, the aerospace industry has experienced a remarkable growth in the use of Unmanned Aerial Vehicles (UAVs) due to their low manufacturing and operational costs, adaptability, and scalability. In the context of climate change and desired emissions targets, UAVs are realistic options to complement the current freight transportation methods, and in the future, as an viable option for human mobility. UAVs are also starting to gain a place in emergency response, both in urban and rural areas, where aid or surveillance capabilities are required in short notice and a fast response is crucial. However, an important obstacle towards their broader use is the expected noise annoyance caused by UAV operations. In this study, we combine extensive outdoor measurements of drone noise with statistical modelling to predict acoustic metrics relevant to determining acoustic annoyance. Array-based measurements combined with GPS positioning information of an eVTOL fixed-wing UAV are studied under realistic operational conditions in an open field. The linear least squares theory is used to establish an empirical model and identify a set of control parameters, including acceleration and velocity, that serve as effective predictors of noise output. The results pave the way for the establishing a model that predicts drone noise for different UAV types and for different operational conditions.

Keywords: Drone noise, Empirical models, Drone operation parameters

1. Introduction

One of the major concerns of a broader implementation of UAVs, both at a commercial and emergency response level, is the reported acoustic annoyance caused by their operations (Eißfeldt & Vogelpohl, 2019), (McKinsey & Company, 2021), (Bajde et al., 2021). Therefore, to produce a successful implementation of UAV-based technologies, it is necessary to address this issue. It is essential to study a broad range of manoeuvres typical of real operations, understanding the connection between flight dynamics, drone attitude, and the acoustic annoyance on the ground, and how they interplay with the weather conditions, wind

in particular. Wind perturbations are known to be important for the operation and thus for the type and level of generated noise.

In this context, it is clear that there is an increasing need for models to predict the acoustic annoyance of UAVs during real operations, allowing for adequate mission planning and optimization of manoeuvres to reduce the annoyance. At the same time, the models have to be representative of different drone types with their acoustic characteristic dynamics, while also being computationally inexpensive to allow for their implementation in optimization frameworks. Several researchers have studied the sound generating mechanisms in propellers and drones in controlled environments (Tinney & Sirohi, 2018; Intaratep, Alexander, Devenport, Grace, & Dropkin, 2016), aiming to understand the fundamentals underlying drone sound generation. However, the impact on acoustic signature for operating in non-controlled environments is not fully understood.

Over the last years, different works have been published approaching the acoustic dynamics of drones under real operations, studying particular UAV operations (Ramos-Romero, Green, Torija, & Asensio, 2023; Konzel & Greenwood, 2022; Zhou, Jiang, & Huang, 2022). In this study, we take a first step towards describing the acoustic performance in real conditions, by developing empirical models based on correlating flight dynamics variables and measured acoustic features.

2. METHODOLOGY

2.1 Experimental data and measurements

To develop noise models for realistic drone operations, it is necessary to collect a large amount of high quality data of the flight dynamics and acoustic features for such operations. Therefore, a measurements campaign was conducted in the Netherlands, in which two microphone arrays were used to measure the emitted sound during the drone flights, while different operational logs were made available after the completion.

One array was manufactured by the company DEMO with 64 microphones, an aperture of 4 m, and a sampling frequency of 50 kHz. The other array is a CAE-manufactured array, with 112 microphones, an aperture of 1 m, and a sampling frequency of 48 kHz.

A hybrid eVTOL UAV was selected from these measurements to develop the tools and models. A photo of the drone is shown in figure 2. The specific drone measurements were selected based on their clear signal to noise ratio and availability of GPS information. This operation contained four recorded approximate flyovers (the drone did not fly directly overhead), that were used as training and validation data for the first modelling approach. In figure 1 the trajectory of this operation can be observed.

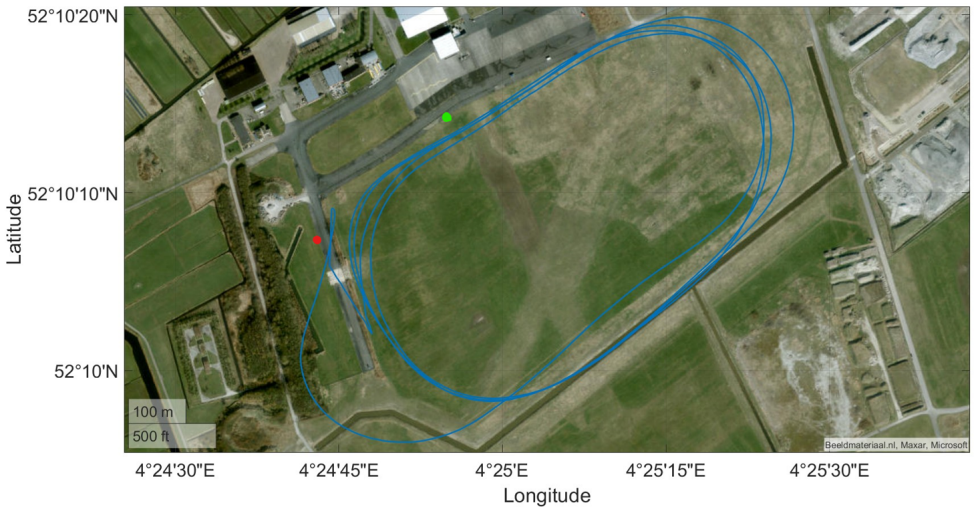

Figure 1: Satellite image of the measurements area. The trajectory of the flight performed by the hybrid eVTOL during the 2023 experimental campaign can be observed (blue). The positions of the DEMO array is represented with the green mark, while the position of the smaller array is represented with the red dot. The data processed in this work is extracted from the main (DEMO) array.

Figure 2: Photo from the eVTOL Avy Aera 3, built by the company Avy. The drone takes off and lands vertically as an octocopter, using the 4 vertical rotors. For forward flight manoeuvres, the horizontal propeller is used while the 4 rotors can also operate if additional trajectory stabilization and manoeuvrability is needed.

The drone operates in a hybrid way; it takes off as a normal quadcopter, and then transitions to horizontal flight activating its horizontal propeller. During these stages, the vertical rotors can still be used to provide more stability or manoeuvrability.

2.2 Tone reconstruction algorithm

To quantify the tonal component of the acoustic signal, a tone reconstruction algorithm was developed using the four flyovers as test data. One of the goals of the algorithm is to reconstruct, from the identified tones, the blade passage frequency (BPF) as a function of time, which in general is a complex task.

The algorithm takes the following four steps to extract the tones of a flyover spectrogram:

- Extraction of broadband component from the spectrum at each time step, i.e., snapshot of acoustic data, considered: The algorithm fits a second-order polynomial and

subtracts it from the main spectrum. In the considered dataset, each time step was 0.1 seconds.

- The fundamental frequency at each time step is determined by finding the frequency that results in maximum correlation with a synthetic noise model.
- The BPF determination is fine-tuned by allowing small variations in the fundamental frequency.
- By identifying harmonics in consecutive time steps whose frequencies are the most similar, the tones are reconstructed from the detection on individual spectra. For each tone the corresponding SPL values, frequencies, and times are determined.

The synthetic noise model was developed aiming to have a mathematically simple form of generating a function whose Fourier transform has a defined fundamental frequency and a number of harmonics. This was done by creating a synthetic function as:

$$S(t, f_0, N_h) = \sum_{n=1}^{N_h} e^{2\pi i n f_0 t} \tag{1}$$

where f_0 is the fundamental frequency and N_h is the number of assumed excited harmonics. This mathematical form ensures that in the frequency space only the peaks at f_0 and its higher harmonics will appear. Note that t is not the snapshot time, but the time within the snapshot. In the above expression, it is assumed that the signal is dominated by a single independent BPF and its harmonics. However, it is straightforward to extend it to cases where more sources (propellers) with different BPFs are present simultaneously.

For a rotating rotor with n_b blades, the rotor's RPM is related to the BPF (f_0 in equation 1) through the following equation:

$$BPF = \frac{RPM * n_b}{60} \tag{2}$$

In the second step, the algorithm varies the value of RPM in a preset range and computes the synthetic spectrum for each value. Naturally, this creates as many synthetic spectra as values of RPM (or BPF), which only differ on the value of the fundamental frequency (and spacing between harmonics). For each of these synthetic spectra, the algorithm then calculates the correlation coefficient with the experimental spectrum. The RPM value that maximises the correlation coefficient is selected as the correct fundamental frequency for that specific time step/spectrum. This process is repeated for all snapshots of the signal.

However, even with a good frequency resolution (i.e. sufficient length of snapshot), in a real signal, consecutive harmonics may not be separated by exactly the fundamental frequency. Therefore, in the third step, the algorithm refines the harmonics detection. This step consists of searching in the close vicinity of each detected harmonic for a higher correlation. This process markedly improves the peak detection, reaching an almost perfect detection for harmonics with amplitudes larger than 20 dB.

Up to this point, the algorithm provides a set of tone SPL values and their frequencies for each time step. However, it was additionally required for the algorithm to output the tones' temporal behavior. This was done by identifying the set of detected harmonics that shared similar frequencies across consecutive time steps. The implicit assumption is that a tone will not change its frequency considerably from one time step to the next. In this context, a considerable frequency change is a variation in the order of the BPF value from one time step to the next.

Finally, the algorithm outputs the following results:

- Tonal SPL per time step
- Tonal frequencies per time step
- BPF per time step
- SPL of each tone
- Frequencies of each tone
- Time steps at which each tone is present.
- Broadband SPL per timestep

2.3 Acoustic localization

Due to the integration of data from different sources, primarily GPS-based and acoustic array-based, it is fundamental to develop a method to synchronize both data sources.

The procedure consisted of localizing the main source of noise using a differential evolution algorithm based solely on the array-based acoustic data (Von Den Hoff, Merino-Martinez, Simons, & Snellen, 2022; Altena, Luesutthiviboon, de Croon, & Snellen, 2023). The output of this algorithm is the most likely position of the sound source, which is then adjusted to match the GPS-based signal. This adjustment yields the time shift that has to be compensated for both datasets to be synchronized. Throughout the process, it was assumed that this offset was constant.

Broadly speaking, genetic algorithms iteratively update a set of unknowns much like genes undergo updates through mutations and crossover across evolutionary cycles via reproduction. The unknowns are in this case the two angles of the drone relative to the array. At each iteration or cycle, realizations of these unknowns are used as inputs for an energy function that quantifies, in this case, the difference between the acoustic signals measured by the array and predicted by a model for a given drone position. The objective is to find the unknowns that minimize the difference. For each iteration, the unknowns are updated via two computational processes denominated mutation and crossover (other processes can also be added). This is done for a fixed number of iterations.

2.4 Least squares-based linear model

The modelling approach aimed to explore the simplest hypothesis that relates flight dynamics parameters to the acoustic features. A linear model is assumed, which means that the relation between the input parameters a_i and an acoustic observable y is linear, given by a scalar x_i. This can be expressed as a linear model $y = Ax$, where a_i is the i^{th} column of the A matrix, and the scalars x_i are the elements of the vector x. In general $y = Ax + e$, where e is the residual vector. The shape of the model equation indicates that each control parameter contributes linearly to the output y.

As with most statistical modelling techniques, there is no a-priori physical interpretation about the x_i. Once the model is stated, the main goal is to estimate (train) the parameters x_i using the experimental data. To estimate x and keep the assumptions as simple as possible, the least squares method was used to perform the fittings and parameter estimations.

For the linear model of the form $y = Ax$, the best linear unbiased estimator of x is

$$\hat{x} = \left(A^T Q_y^{-1} A\right)^{-1} A^T Q_y^{-1} y \tag{3}$$

where Q_y is the variance-covariance matrix of the acoustic observable y. Since the measurements are assumed uncorrelated with identical precision, Q_y is a diagonal matrix with identical values of 2 dB, which corresponds to the sensitivity of the DEMO array.

This formula ensures that the estimated parameters will be the best estimate possible given a least squares problem, i.e, the parameters that give the least possible value of the weighted quadratic form of the residuals. To test the discrepancies between observed data and assumed model, the following test statistics, referred to as the overall model test, can be used:

$$||\hat{e}||^2_{Q_y^{-1}} = \hat{e}^T Q_y^{-1} \hat{e} \tag{4}$$

where $\hat{e} = y - A\hat{x}$ is the estimator of the errors; the vector difference between the acoustic observable y and the estimated observations $\hat{y} = A\hat{x}$ obtained from the linear model.

3. RESULTS

3.1 Summary of obtained data

During the measurements campaign aforementioned a range of operations were flown by different systems. The flight plans were determined mostly by each operator, however, most of them performed level flights which were recorded by the microphone arrays. Additionally, in some cases, the landing and take off were also recorded. In the table below, a summary of the drones, their types, masses and type of acquired data is shown.

Table 1: Table with a summary of the measured drones, their type, and the available experimental data.

UAV	Type of drone	MTOW [Kg.]	Measured data
Avy Aera 3	eVTOL fixed-wing	12	Acoustic data and GPS
Dronevolt H20	Coaxial octopter	26	Acoustic data, GPS, and RPMs
DJI M300	Quadcopter	9	Acoustic data and GPS
Altura Zenith	Coaxial octopter	6.5	Acoustic data and GPS
Atmos Marlyn	eVTOL fixed-wing	6.7	Acoustic data and GPS
Custom-made drone	eVTOL fixed-wing	-	Acoustic data
Several FPV drones	Quadcopters	-	Acoustic data

3.2 Initial acoustic analysis

All four flyovers belonging to the selected ANWB flight present broadband and tonal noises, whose spectral content can be observed in figure 3. In particular, clear tonal noise can be observed between 50 Hz and 8 kHz, with two distinct harmonic contributions between 50 Hz and 7 kHz, and between 6.5 kHz and 9 kHz, as it can be observed in detail in figures 3, where one spectrogram was used as an example of these dynamics.

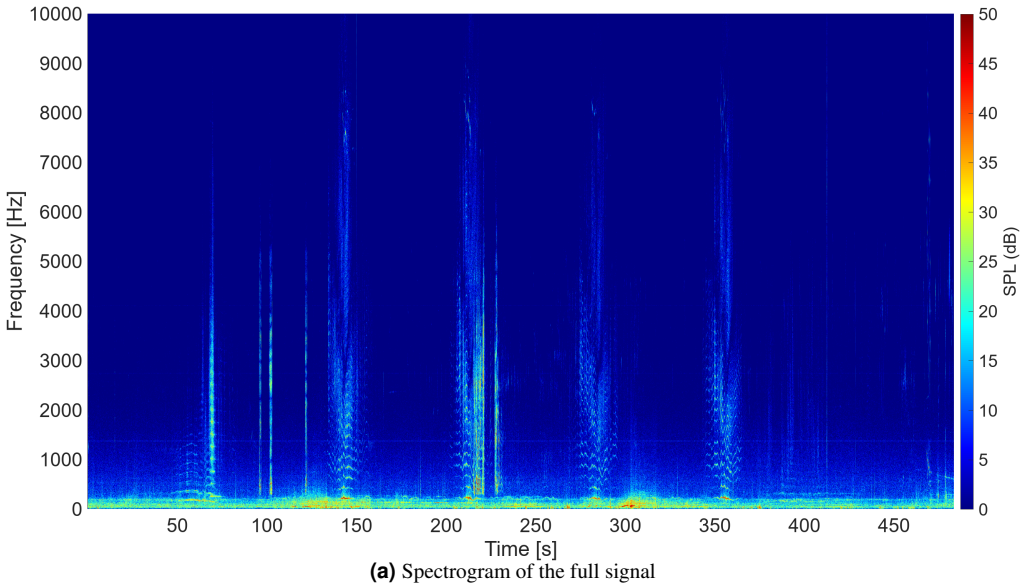

(a) Spectrogram of the full signal

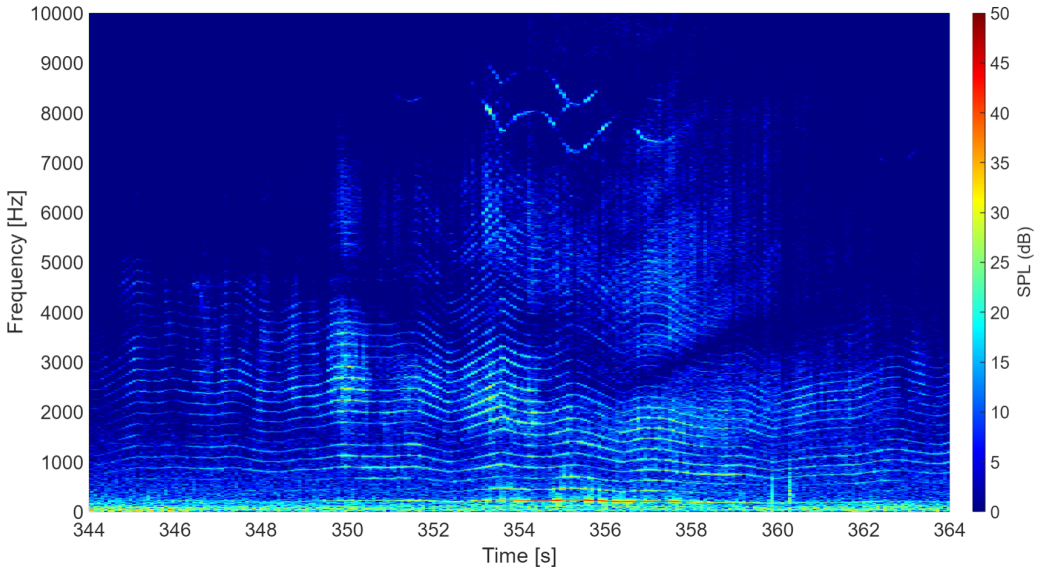

(b) Spectrogram of last flyover

Figure 3: Single-microphone spectrogram of the complete signal, including the detail of one of the level flights (called flyovers herein forth). During the operation, four instances of level flight were performed close to the microphone array. From the detailed spectrogram (b), the signal contains two tonal contributions and broadband noise. The tonal component present between 100 Hz and 7000 Hz corresponds to rotor noise, and another contribution between 7000 Hz and 9000 Hz, which is thought to be due to the internal engines activity. Additionally, broadband noise was also found in the entirety of the flyover signals.

During flight, there were 4 flyover instances, where ideally the horizontal propeller keeps a constant activity without assistance from the rotors to keep a level flight at constant speed.However, it is seen that the tonal dynamics is not constant and the tones are not occurring at a constant frequency in time. This is partially (at this point, it could not be assured that there were no other factors of interests) due to the drone flying under windy conditions, which causes the control system to adapt the RPM of the propeller and of each rotor to maintain the programmed trajectory, which in turn causes the variable frequency dynamics observed in the spectrogram.

The tonal contribution visible from 50 Hz to 8 kHz is due to the rotors activity (either the propeller or the vertical rotors, or a combination of both), whose tonal excited frequencies occur at the blade passage frequencies (BPF) and their harmonics. Based on observations from previous research, the contributions at the higher frequency bands between 6.5 kHz

and 8 kHz is hypothesized to be due to engine noise (Huff & Henderson, 2018; Henderson, Huff, Cluts, & Ruggeri, 2018). In addition, it could also be observed that more than one independent BPF (and their harmonics) are present at some time instances, but with less amplitude.

There is also a region of attenuation in the frequency range of 2 kHz and 4 kHz. In order to understand if this was an error in the selected microphone, a pair-wise correlation study between all pairs of microphones was conducted considering the SPL of each tone (data not shown). This study showed an almost perfect correlation between all microphones, which means that all the microphones measured approximately the same attenuation effect at the same frequencies and times. It is hypothesized that this attenuation stem from reflections at the metal structure of the array.

3.3 Tonal noise reconstruction

The tone reconstruction algorithm was used to obtain the tonal dynamics. Figure 4 shows the reconstructed tones for the flyover spectrogram presented in figure 3.

The reconstruction process needed a proper resolution of the RPM search range; a too coarse resolution might lead to the algorithm not finding the proper BPF, while a very fine resolution might lead to a high computation time. A resolution of 12 Hz was chosen, which is in the range of the frequency resolution of the signal, with a BPF search range from 130 Hz to 250 Hz. The total computation time of the algorithm was around 15 to 20 minutes on a single processor to provide the full reconstruction for flyover signals with duration ranging from 10 to 20 seconds.

After several sensitivity studies, where the input parameters were changed, we found that the algorithm performance depends almost exclusively on proper resolutions of the RPM search range and the selected frequency bands. However, the dependency on the frequency range itself did not affect the performance of the reconstruction. The algorithm was tested on signals with different ranges of fundamental frequencies (80 Hz up to 250 Hz) and broadband contributions, and it was able to reconstruct the tones in all cases.

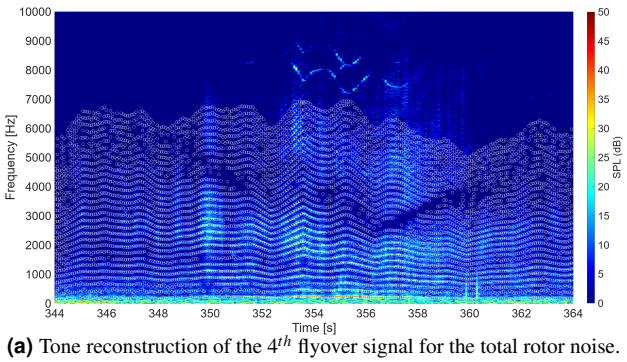

(a) Tone reconstruction of the 4^{th} flyover signal for the total rotor noise.

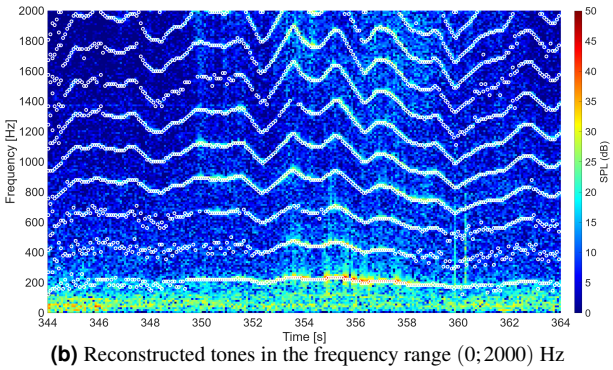

(b) Reconstructed tones in the frequency range $(0;2000)$ Hz

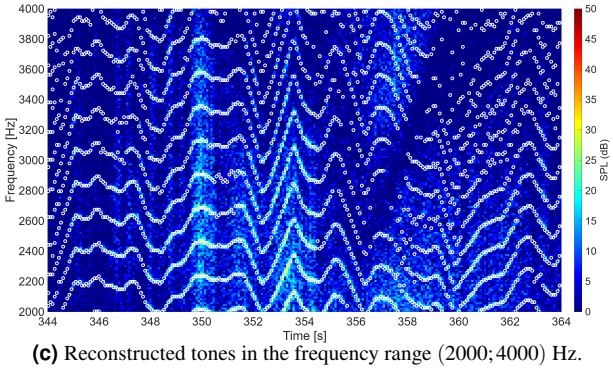

(c) Reconstructed tones in the frequency range $(2000;4000)$ Hz.

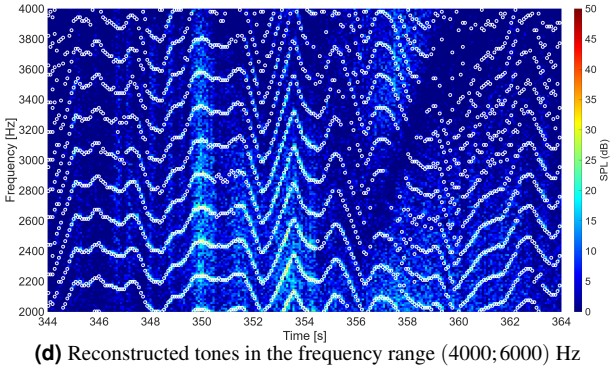

(d) Reconstructed tones in the frequency range $(4000;6000)$ Hz

Figure 4: Results from the tone reconstruction algorithm for one of the flyovers. The algorithm was applied to extract the rotor tonal activity between 150 Hz (approximate value of the BPF), and 7000 Hz. It can be observed that the reconstruction is accurate throughout the mentioned frequency range, with a resolution of 12 Hz. The algorithm returns the amplitude (SPL value), frequency and times of each of the tones, however, for visual clarity purposes, only the frequency and time reconstruction are included in this figure. The inaccuracies observed for some of the reconstructed tones arise from the low experimental SPL values at those times. It was observed that by establishing a minimum detection threshold of 20 dB, the resulting reconstructed tones are highly precise and no inaccuracies are found throughout all the flyover events.

To check the reconstructed BPF signal, the cepstrum of the signal was computed (Bogert, Healy, & Tukey, 1963; Norton & Karczub, 2003). Since the signal was highly fluctuating and there are more than one BPF present at certain times, the cepstrum does not hold a unique peak but many. Therefore, it is not possible to use it as an alternative to estimate the fundamental frequency a priori, however, it can be used a posteriori to check whether there is a local maximum in the quefrency domain around the area where the BPF was detected using the reconstruction algorithm. The result of this analysis can be observed in figure 5 for a fragment of the signal.

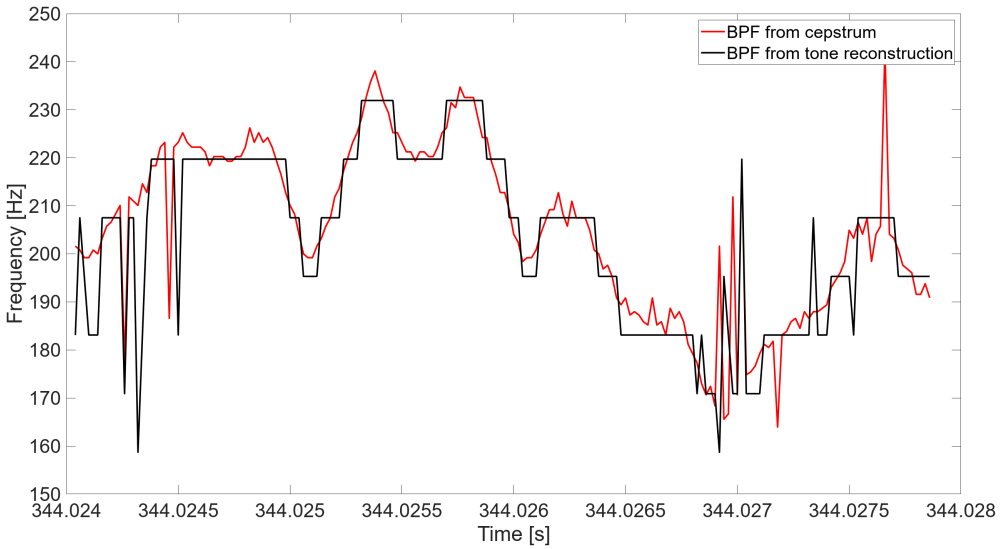

Figure 5: Comparison of the BPF values obtained with the reconstruction algorithm and with the cepstrum. It is possible to observe that the reconstruction and the cepstrum follow similar trends. However, the cepstrum presents many fluctuations caused by the relative intensity of the main peaks being low. This causes many difficulties when developing a systematic way of identifying fundamental frequencies for all the timesteps based on cepstrum.

From the comparison with the cepstrum, it can be observed that the reconstruction algorithm does detect a fundamental frequency consistent with one local maximum in the quefrency space. It is worth mentioning that the accuracy of the fundamental frequency estimation from the cepstrum varies in time and depends greatly on the explored quefrency range, since the local maximum criteria does not always hold accurate results due to the different BPFs and fluctuations present.

3.4 Acoustic features

Once all the tones were reconstructed for all flyovers, acoustic features are calculated from the measurements to generate the different y vectors for $y = Ax$. A set of features was then generated to cover different aspects of the sound (in addition to the outputs from the tone reconstruction):

- $OSPL$: Classic overall sound pressure level, calculated using the tonal component of the signal, providing a metric of the total energy per time.
- SPL dispersion in time (σ_{SPL}): This metric is calculated from the distribution of SPL at each time step. In particular, at time step t_i, the $SPL_k(t_i)$ for all tones $k = 1,2,...,N$ are identified. The SPL distribution $\rho_{t_i}(SPL)$ is calculated at each time step, where $\rho_{t_i}(SPL)\Delta(SPL)$ represents the number of harmonics that have their SPL values between SPL and $SPL+\Delta(SPL)$. Then, σ_{SPL} is the standard deviation of the distribution $\rho_{t_i}(SPL)$ at time step t_i. The metric was calculated as a measure of how different the energy among all the excited harmonics is at each time step.
- Number of tones (n_{tones}, n_T): This metric is the number of tones that have their energy above a given threshold. For this study, a threshold of 10 dB was chosen.

The information from $\sigma_{SPL}(t)$ and $n_T(t)$ gives a representation of how dispersed the tonal energy is as a function of time. In figure 6, examples of the three features for one of the flyovers can be observed.

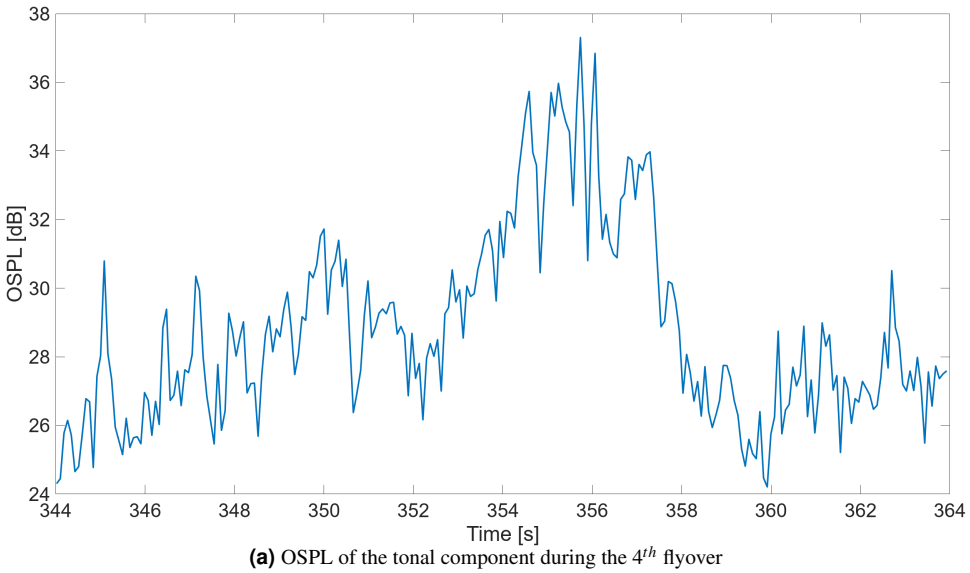

(a) OSPL of the tonal component during the 4^{th} flyover

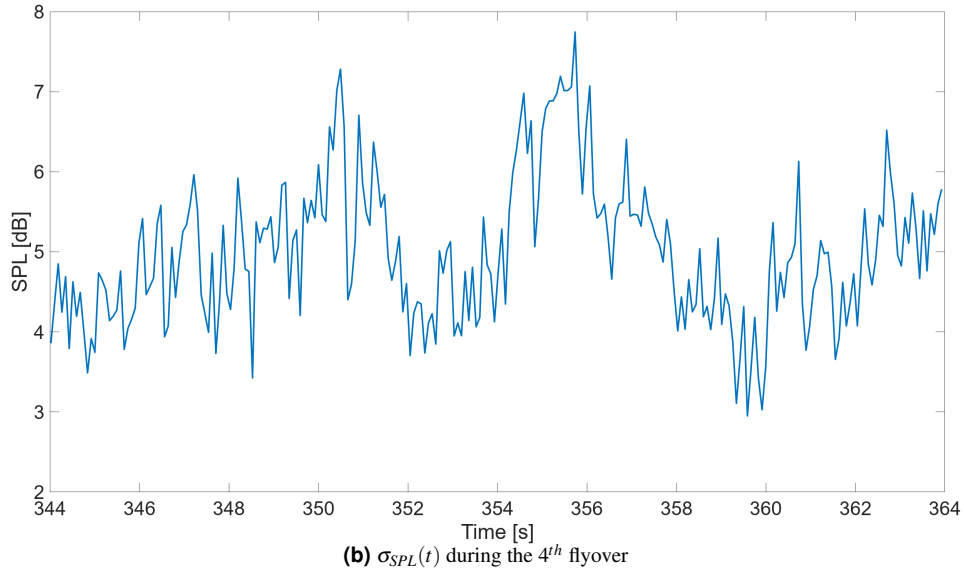

(b) $\sigma_{SPL}(t)$ during the 4^{th} flyover

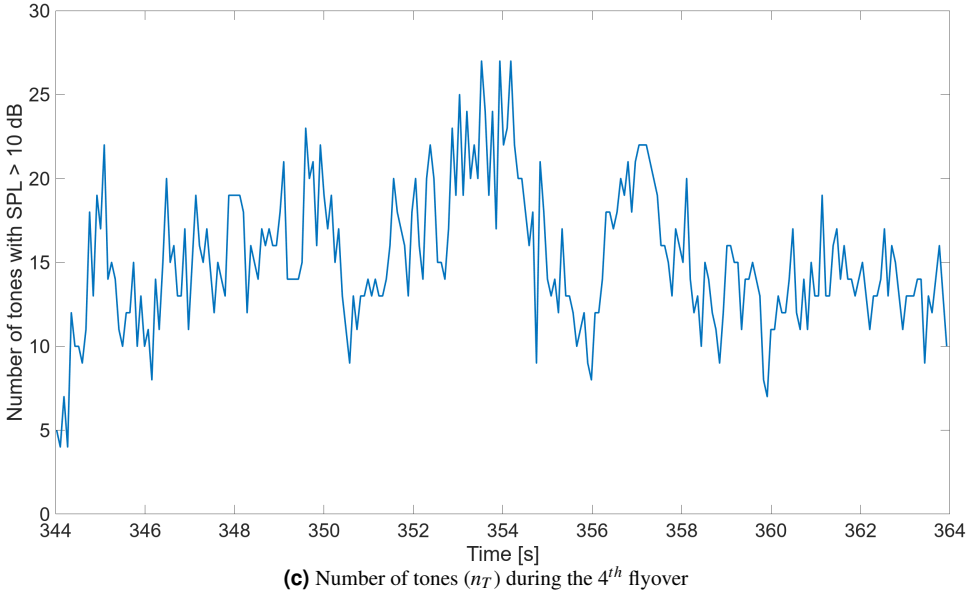

(c) Number of tones (n_T) during the 4^{th} flyover

Figure 6: (a): OSPL as a function of time for the 4^{th} flyover.(b) Standard deviation of tonal power as a function of time. A low value of the observable indicates that the excited tones have similar amplitudes, whereas a high value represents the case when the excited tones have very different energies. (c) Number of tones with $SPL \geq 10dB$ as a function of time. These features allow for a characterization of the tonal spectral content, representing total energy and its distributions in time.

3.5 GPS-array synchronization: Acoustic localization

To synchronize the times from the GPS and the acoustic data, the elevation angles from the GPS and acoustic localization were computed, which can be observed in figure 7. This angle is built in such a way that $\theta = 90°$ when the drone is overhead, and $\theta \to 0°$ when the it is close to the horizon.

In figure 7, the dynamics of both signals are similar which was used to determine the delay. However, it is also possible to observe that the absolute values of both datasets differ. Despite this, the similarity between the shape of both signals allowed for an estimation of the delay with an uncertainty arising from the mismatch between absolute values. In figure 7, the signals after compensating for this delay can be observed. Importantly, the synchronization procedure also conserves the travelling times from the drone (synchronized GPS times) to the array (acoustic times), which is considered in a later stage after both signals are matched.

It is also clear that the performance of the applied acoustic localization was not reliable below $\theta = 17°$, where highly fluctuating values were obtained.

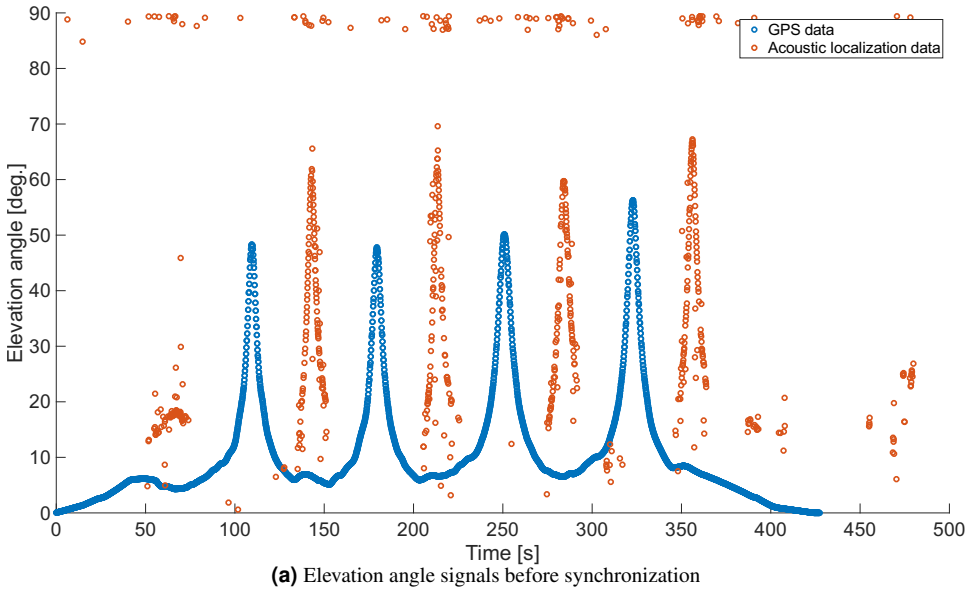

(a) Elevation angle signals before synchronization

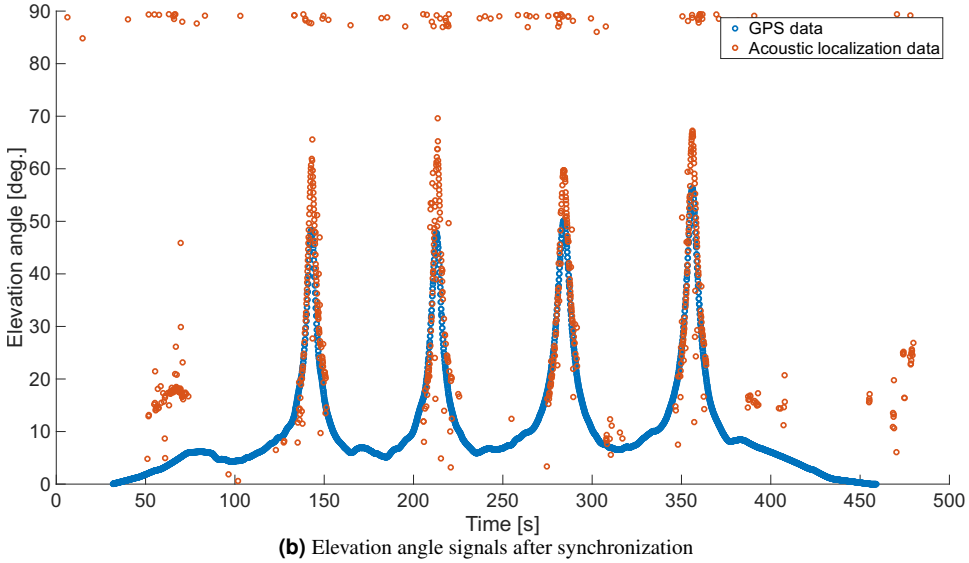

(b) Elevation angle signals after synchronization

Figure 7: Elevation angle as a function of time calculated from the GPS position and from the acoustic localization. Assuming a constant non-physical delay between both signals, the synchronization was accomplished by finding the factor for which both signals coincided.

3.6 Classic least squares linear model

Employing the least squares-based linear model introduced in the previous sections, a linear model was developed as a first modelling approach. In the formalism, a fixed form of the A matrix is assumed, however, the adequate combination of control parameters is not known. Therefore, to decide the best A matrix, i.e, the most adequate set of control parameters, a procedure was developed based on the least squares formalism.

The possible input (feature) parameters for constructing the A matrix were:

- $-20\log(r)$: This parameter is responsible for the spherical spreading of the sound wave (in logarithmic scale given that the output parameter is expressed in terms of SPL). r is the distance between each point of the drone trajectory and the array.
- $-r$: This parameter reflects the expected atmospheric absorption effect.
- $\bar{v}$: The drone velocity vector, computed from the GPS data.
- $\bar{a}$: The drone acceleration vector, computed from the GPS data.
- θ and ϕ: The elevation and polar angles describing the drone angular position relative to the array. These were added in order to account possible effects arising from the source directivity hemisphere. These signals were computed from the GPS data as well.

A constant control parameter was also added to account for offsets between the input and output signals. Importantly, the components of the vectors $\bar{v}$ and $\bar{a}$, as well as their norms were considered separately, to allow for additional relevant combinations.

The statistics $||\hat{e}||^2_{Q_y^{-1}}$ was used to assess the best combination of control parameters, computing it for all the possible A matrices. This process was done for the four flyovers of the dataset to find the best combination of parameters and training data. The combination that minimized $\hat{e}^T Q_y^{-1} \hat{e}$ was considered to be the most adequate set of control parameters. This process was done for the cases where the acoustic observable was the $OSPL$, the σ_{SPL}, and n_T. Importantly, in all cases the statistics $||\hat{e}||^2_{Q_y^{-1}}$ is computed adding a normalization to account for the different amount of data in each flyover, therefore, it is always used as $||\hat{e}||_n := \frac{||\hat{e}||^2_{Q_y^{-1}}}{d.o.f}$, where $d.o.f$ is the degrees of freedom of the model, with $d.o.f = n-k$, where n is the number of data points and k is the number of parameters, only added when training is being evaluated.

The result of this study indicated that initially the best linear models contained the following control parameters for all features, with different values of the estimated parameters $\hat{x}$ for each of them.

$$b_0 + b_1(-r) + b_2(-20\log(r)) + \sum_{i=1}^{3} c_i|v_i| + \sum_{i=1}^{3} d_i|a_i| \tag{5}$$

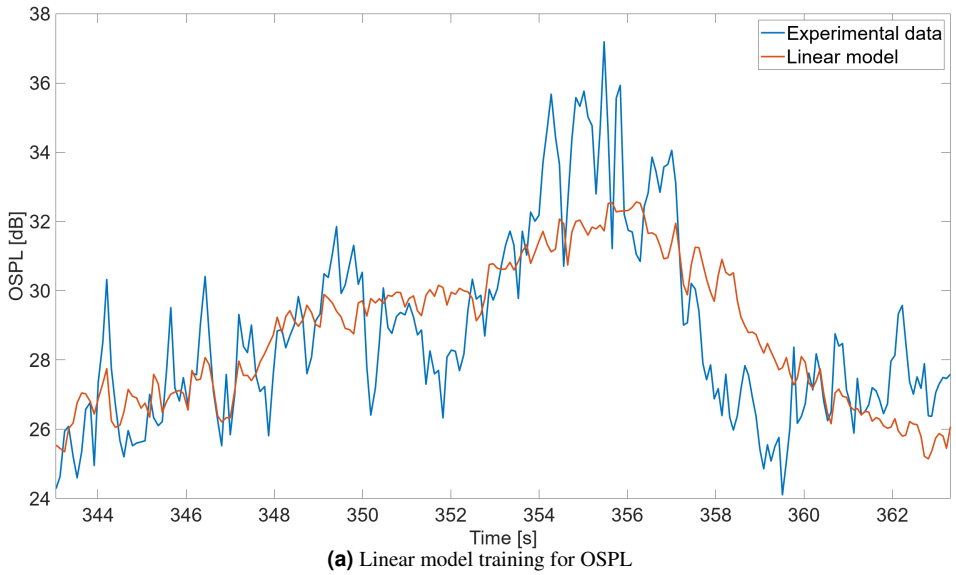

(a) Linear model training for OSPL

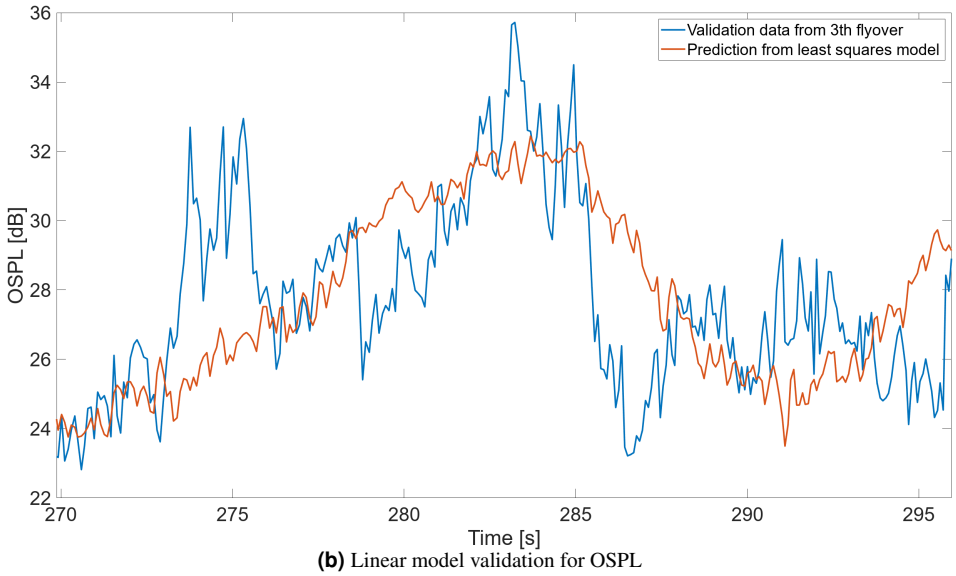

(b) Linear model validation for OSPL

Figure 8: OSPL model performance. In (a), the linear model parameters training can be observed, where the model manages to reconstruct the trend of the signal for most times, but it does not fit the absolute values. This behavior is kept throughout the validation results. For some times, it was observed that the model does not manage to trace sudden changes in OSPL, which can be seen around the main crest of the different signals.

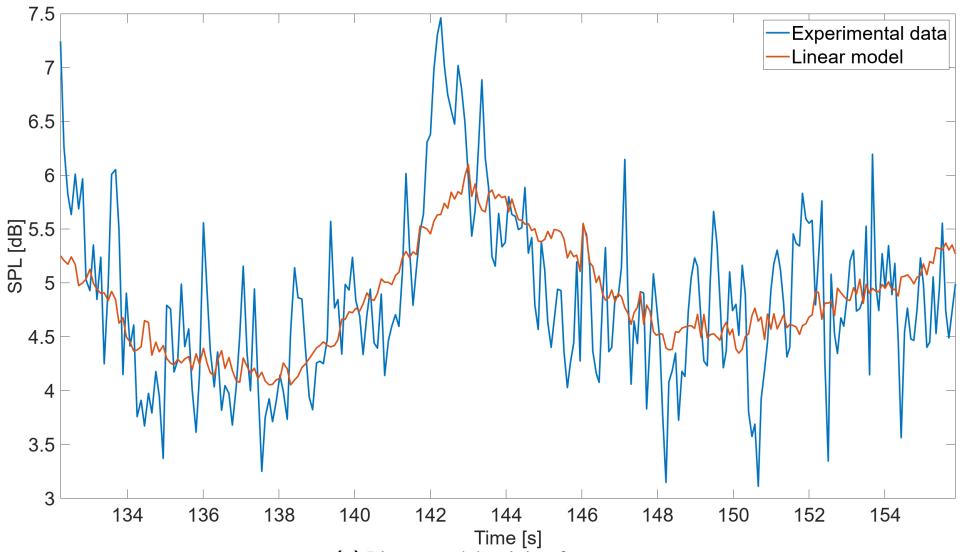

(a) Linear model training for σ_{SPL}

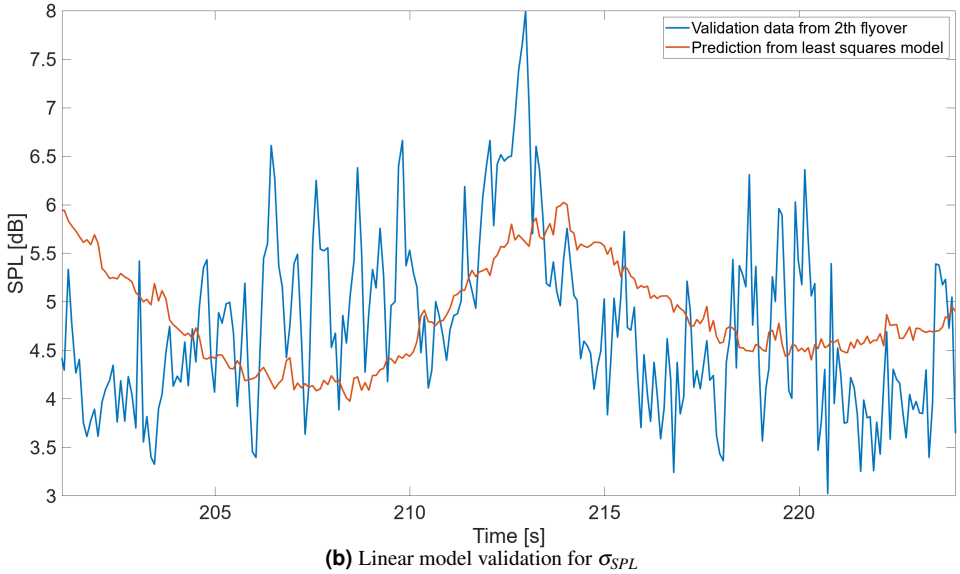

(b) Linear model validation for σ_{SPL}

Figure 9: σ_{SPL} model performance. The trend of the signals is successfully captured except towards the beginning and ending of the signal, where it is consistently observed throughout all the flyovers that the model and the data differ, with the model prediction overestimating the values of σ_{SPL}. In this case, it was also observed that the peaks from the model and experimental data do not coincide temporally.

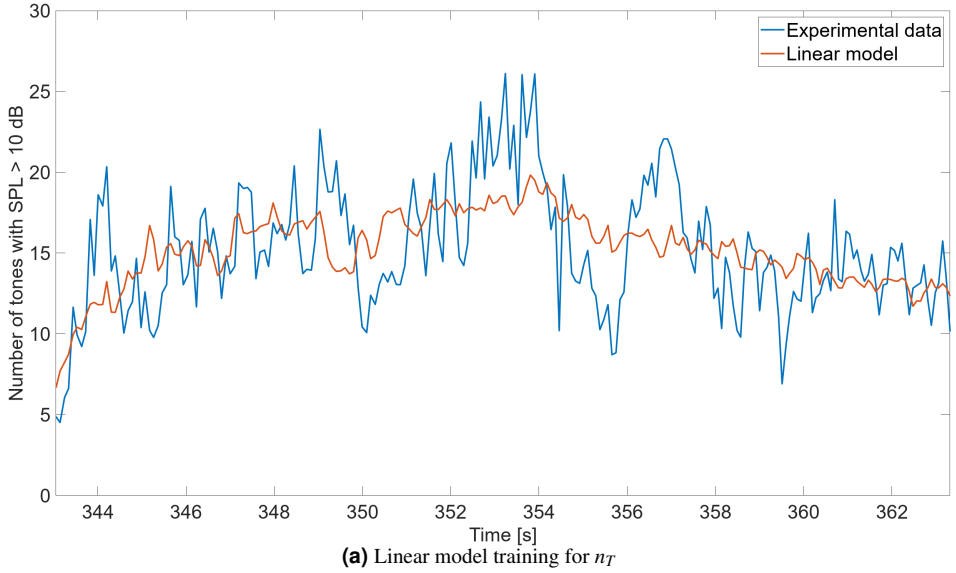

(a) Linear model training for n_T

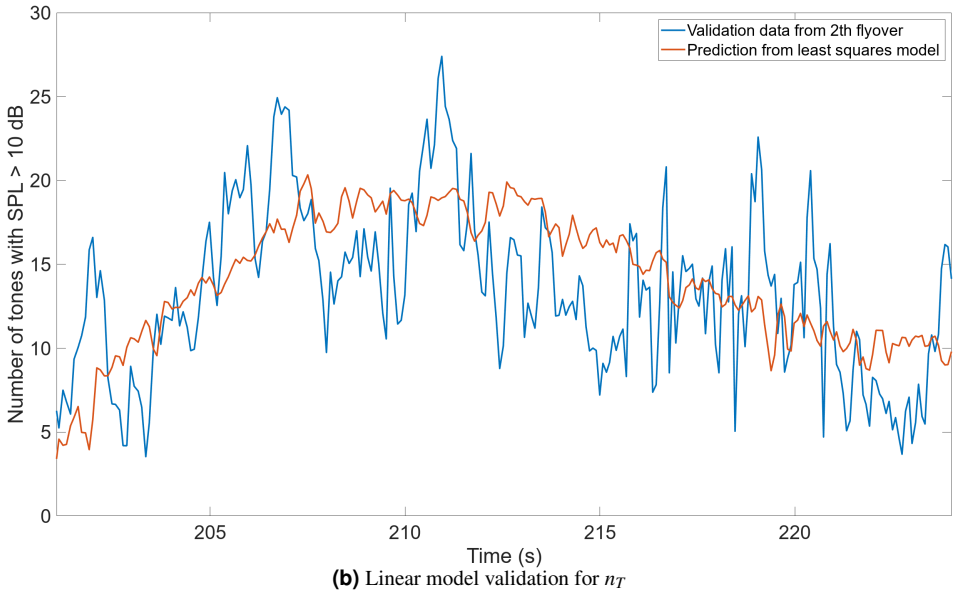

(b) Linear model validation for n_T

Figure 10: n_T model performance. In this case, the observable has a more stable trend presenting less prominent peaks than in the previous two cases. The model again does not describe the absolute values.

In the case of the OSPL, from the different validations it is seen that the model manages to fully capture the behavior when a single crest is found in the data, similarly to the one plotted in figure 5a. However, in cases when an event has more maxima, such as the one in figure 8b, the model has issues reproducing the complete trend.

The model performance of σ_{SPL} presents a better agreement, with the trends better captured throughout all of the flyover. In some cases, differences are observed towards the beginning and end of each signal, when the model tends to overestimate the values of σ_{SPL}, which might be due to overfitting issue during the training process in those parts.

In case of n_T, the model manages to capture the trends in all events, while the absolute values however are still not described with this framework, even in the case of a signal with less prominent crests.

Overall, from figures 8, 9, and 10, it is clear that the models only managed to reproduce the overall trends with some large variations at some time steps, while they do not reproduce absolute values. However, this indicates potentially relevant variables to describe the average behavior of the presented features in the considered manoeuvres. Therefore, in order to assess which parameters are statistically relevant for these dynamics, a hypothesis test was developed.

For each estimated parameter $\hat{x}_i$, we test whether the parameter is statistically significant at the 95% confidence level. As the null hypothesis assumes that the parameter is not significant, this hypothesis is accepted if zero is contained in the following confidence interval: $(\hat{x}_i - k_{\frac{\alpha}{2}}\sigma_{\hat{x}_i},\ \hat{x}_i + k_{\frac{\alpha}{2}}\sigma_{\hat{x}_i})$, where, $\alpha = 0.05$, $k_{\frac{\alpha}{2}} = 1.96$ is the critical value obtained from the standard normal distribution, and $\sigma_{\hat{x}_i} = \sqrt{(Q_{\hat{x}})_{ii}}$ is obtained from the diagonal elements of the variance-covariance matrix of the estimated parameters, i.e. $Q_{\hat{x}} = (A^T Q_y^{-1} A)^{-1}$. These analysis led to the statistical significant model for each observable to be:

$$OSPL = \alpha_0 + \alpha_1(-r) + \alpha_2(-20\log(r)) + \alpha_3|v_y| + \alpha_4|v_z| + \alpha_5|a_z| \tag{6}$$

and

$$\sigma_{SPL} = \beta_0 + \beta_1(-r) + \beta_2(-20\log(r)) \tag{7}$$

and

$$n_T = \gamma_0(-20\log(r)) + \gamma_1 v_x + \gamma_2 v_y + \gamma_3 v_z + \gamma_4 a_y + \gamma_5 a_z \tag{8}$$

This study indicates that not all the control parameters found with the least squares method are relevant to accomplish the observed fitting and predictions. In particular, the statistically significant A matrix for each feature was different, even if the initial sets of control parameters were the same, as shown in equation 5.

4. Discussion

A measurement campaign was conducted during which several operations from different drones were recorded, with GPS information available from most of them. From this database, a dataset was selected to generate the first analysis tools and models. A tone reconstruction algorithm was developed that successfully extracts the tones (amplitudes, frequencies, and times) throughout all the dataset with a high level of accuracy for $SPL > 20dB$. The algorithm can also estimate the broadband contribution relative to the total SPL, however, based on the tonal nature of the selected dataset, this has not been further explored for this particular vehicle. Overall, the algorithm works well when there is a single dominant BPF present, which is expected mostly during hovering and take-off, where all the rotors are approximately working at the same RPMs. Since a full flight envelope should in general be studied, the algorithm is being extended to address more general cases without relying on the single BPF assumption. It can also be adapted to the scenarios where broadband noise is the main contributor.

Using the information obtained from the extracted tones, several acoustic feautures were calculated to be used as output for the linear model, which is able to capture some of their trends.In terms of the found parameters, and consistently with observations from previous works, the spherical spreading is the most important parameter as it is statistically significant in all three models. In the same sense, this term is not sufficient and other control parameters are needed, such as specific components of the velocity and acceleration vectors.

Several causes were identified behind the disagreements between the linear model and the dynamics of the studied features. The synchronization between the GPS and the acoustic data has a high impact on the quality of the fitting process. It was found that small inaccuracy in the estimation of the delay lead to less accurate training and validations, since the control parameters are shifted relative to the outputs. This is directly related to the quality of the acoustic localization method, which is sometimes hampered by the presence of other sources during the measurements acquisition.

Additionally, the lack of ground RPM data is also an important factor affecting the model performance, since the rotor activity is known to be one of the key factors in the generation

of tonal noise. This could potentially be supplemented by the BPF reconstruction from the presented algorithm; however, ground RPM data is still needed to produce a control dataset.

Since the goal was to explore the simplest hypothesis, a linear model was developed using the least-squares method to estimate the parameters. However, the model has limitation in terms of both the proportionality relations between input and output variables, as well as in the parameter estimation. The linear least squares models are known to capture the linear fluctuations of the features. However, any non-linearity in the features can be better captured using modern estimation methods such as deep learning techniques.

ACKNOWLEDGMENTS

The authors are grateful to the EC for supporting the present work, performed within the REFMAP project, funded by the European Union's Horizon Europe research and innovation programme under grant agreement no. 101096698 (REFMAP). This publication solely reflects the authors' view and neither the European Union, nor the funding Agency can be held responsible for the information it contains. We also want to thank Unmanned Valley and ANWB for facilitating and coordinating the measurements. The authors would also like to thank Anique Altena and Dr. Salil Luesutthiviboon for their efforts during the organization and conduction of the measurements campaign.

REFERENCES

Altena, A., Luesutthiviboon, S., de Croon, G., & Snellen, M. (2023). Comparison of acoustic localisation techniques for drone position estimation using real-world experimental data. *29th International Congress on Sound and Vibration (ICSV)*.

Bajde, D., Woermann, N., Bruun, M. H., Gahrn-Andersen, R., Sommer, J. K., Nøjgaard, M., ... Bucher, J. H. (2021). Public reactions to drone use in residential and public areas. *Available from: https://vbn.aau.dk/en/publications/public-reactions-to-drone-use-in-residential-and-public-areas*, *University of Southern Denmark / Aalborg University*.

Bogert, B. P., Healy, J. R., & Tukey, J. W. (1963). The quefrency analysis of time series for echoes: Cepstrum, pseudo-autocovariance, cross-cepstrum, and saphe cracking. *Proceedings of the Symposium on Time Series Analysis*, 209-243.

Eißfeldt, H., & Vogelpohl, V. (2019). Drone acceptance and noise concerns — some findings. *20th International Symposium on Aviation Psychology*, *NASA, NASA/TP-202005007433*.

Henderson, S., Huff, D. L., Cluts, C., & Ruggeri, C. (2018). Electric motor noise from small quadcopters: Part ii – source characteristics. *AIAA/CEAS Aeroacoustics Conference*.

Huff, D. L., & Henderson, S. (2018). Electric motor noise from small quadcopters: Part i – acoustic measurements. *AIAA/CEAS Aeroacoustics Conference*.

Intaratep, N., Alexander, W. N., Devenport, S. M., Grace, S. M., & Dropkin, A. (2016). Experimental study of quadcopter acoustics and performance at static thrust conditions. *22nd AIAA/CEAS Aeroacoustics Conference*, *2873*. doi: https://doi.org/10.2514/6.2016-2873

Konzel, N., & Greenwood, E. (2022). Ground-based acoustic measurements of small multirotor aircraft. *Vertical Flight Society's 78th Annual Forum Technology Display*. doi: https://doi.org/10.4050/F-0078-2022-17435

McKinsey, & Company. (2021). Study on the societal acceptance of urban air mobility in europe. *Available from: https://www.easa.europa.eu/en/full-report-study-societal-acceptance-urban-air-mobility-europe*.

Norton, M. P., & Karczub, D. G. (2003). Fundamentals of noise and vibration analysis for engineers.

Ramos-Romero, C., Green, N., Torija, A. J., & Asensio, C. (2023). On-field noise measurements and acoustic characterisation of multi-rotor small unmanned aerial systems. *Aerosp. Sci. Technol.*, *141*(108537). doi: https://doi.org/10.1016/j.ast.2023.108537

Tinney, C. E., & Sirohi, J. (2018). Multirotor drone noise at static thrust. *AIAA Journal*, *56*(7). doi: https://doi.org/10.2514/1.J056827

Von Den Hoff, B., Merino-Martinez, R., Simons, D. G., & Snellen, M. (2022). Using global optimization methods for three-dimensional localization and quantification of incoherent acoustic sources. *JASA Express Letters*, *2 (5)*(054802). doi: 10.1121/10.0010456

Zhou, T., Jiang, H., & Huang, B. (2022). Quad-copter noise measurements under realistic flight conditions. *Aerosp. Sci. Technol*, *124*(107542). doi: https://doi.org/10.1016/j.ast.2022.107542